Effective grating theory for resonance domain surface-relief diffraction gratings

Michael A. Golub and Asher A. Friesem

Department of Physics of Complex Systems, Weizmann Institute of Science, Rehovot 76100, Israel

Received August 3, 2004; revised manuscript received December 15, 2004; accepted December 15, 2004

An effective grating model, which generalizes effective-medium theory to the case of resonance domain surface-relief gratings, is presented. In addition to the zero order, it takes into account the first diffraction order, which obeys the Bragg condition. Modeling the surface-relief grating as an effective grating with two diffraction orders provides closed-form analytical relationships between efficiency and grating parameters. The aspect ratio, the grating period, and the required incidence angle that would lead to high diffraction efficiencies are predicted for TE and TM polarization and verified by rigorous numerical calculations. © 2005 Optical Society of America

OCIS codes: 050.1950, 050.1970, 260.1960, 260.2110, 050.2770, 050.1380.

1. INTRODUCTION

Effective-medium theory is currently widely exploited for the analysis of surface-relief subwavelength gratings, whose period is lower than the wavelength of the incident light.[1–3] In this theory, the actual refractive index of the grating grooves is replaced by an averaged, effective index of refraction. Consequently, the light of the zero diffraction order behaves the same as that refracted from a uniform layer with the effective refractive index, while all other diffraction orders are evanescent. For surface-relief gratings in the resonance domain, where the grating period is comparable with that of the illumination wavelength,[4–6] the first diffraction order, rather than the zero diffraction order, becomes dominant. Such gratings are particularly important for such applications as specialized diffractive optical elements,[6,7] ultrashort laser pulse shaping,[8] planar optics,[9,10] grating-waveguide structures,[11] optical communications,[12] and spectroscopy.[13]

To analyze resonance domain surface-relief gratings, it is usually necessary to resort to extensive numerical methods of rigorous diffraction theory.[14–23] In general, these numerical methods deal with fixed grating parameters. Consequently, it is difficult to optimize the various grating parameters and establish trade-offs in order to obtain the best diffraction efficiencies from such resonance domain surface-relief gratings. The physical nature of the unusually high diffraction efficiency in resonance domain surface-relief gratings is not yet understood completely, but there is some experimental evidence to indicate a form of Bragg behavior,[5,24] which is usually attributed only to volume hologram gratings.

In this paper, we present a new approach for analyzing and designing resonance domain surface-relief gratings. It is based on replacing the surface-relief gratings with an "effective and averaged" sinusoidal graded-index grating model.[25,26] The model allows us to obtain a general, analytic, closed-form solution for evaluating the performance of surface-relief gratings with arbitrary groove profiles and high diffraction efficiencies. Moreover, it explains the unusually high diffraction efficiency of gratings in the resonance domain and provides constraints on the grating parameters for which such high diffraction efficiencies can be achieved. The development of our model involves the application of analytical Bragg diffraction equations[27,28] to each infinitesimally thin sublayer of surface-relief grating and analyzing consecutive field propagations along the effective slant direction of the grooves. Our analytic results are then compared with those from rigorous coupled-wave analysis (RCWA) for various surface-relief gratings, showing good agreement.

2. RELATION BETWEEN SURFACE-RELIEF GRATINGS AND GRADED-INDEX GRATINGS

In this section, we first develop the basic relations for comparing the surface-relief grating groove profiles with those of graded-index sinusoidal gratings (just like volume gratings) oriented in various directions. Then we develop the coupled-wave equations for light field propagation in each sublayer within grating groove depth as well as for the overall grating layer.

A. Directionally Averaged Gratings

We begin by considering a basic transmission lossless dielectric surface-relief grating on a planar substrate that is illuminated with a monochromatic oblique plane wave of wavelength λ at an incidence angular orientation of θ_{inc} in a classical mounting. The relevant parameters and geometry of two grooves from such a grating are depicted in Fig. 1. Figure 1(a) shows the actual geometry and parameters. The refractive index of the groove material is n_M, the refractive index of the upper layer (superstrate) is n_i, and the refractive index of the lower layer (substrate) is n_{sub}. The period of this grating is Λ, the maximum depth of grooves measured in the direction normal to the planar substrate is h, and the grooves are, in general, slanted for

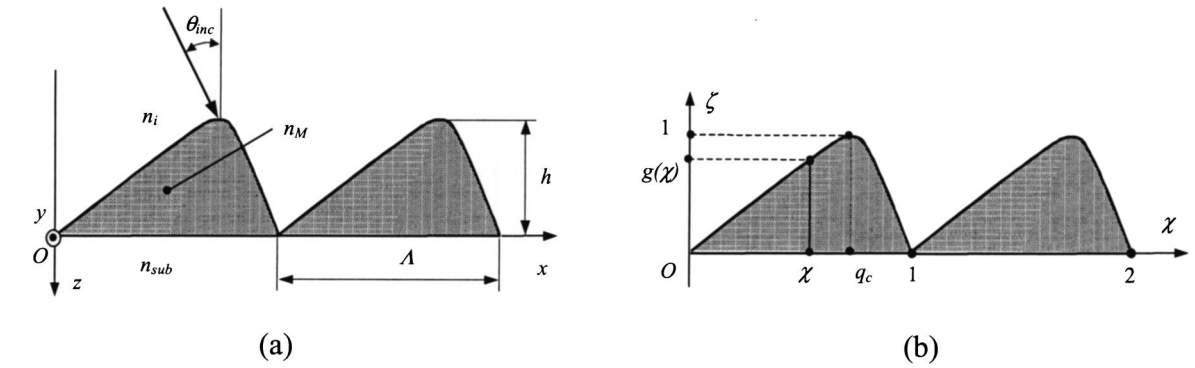

Fig. 1. Relevant parameters and geometry of two grooves from a surface-relief grating: (a) actual geometry and parameters, (b) normalized geometry and parameters.

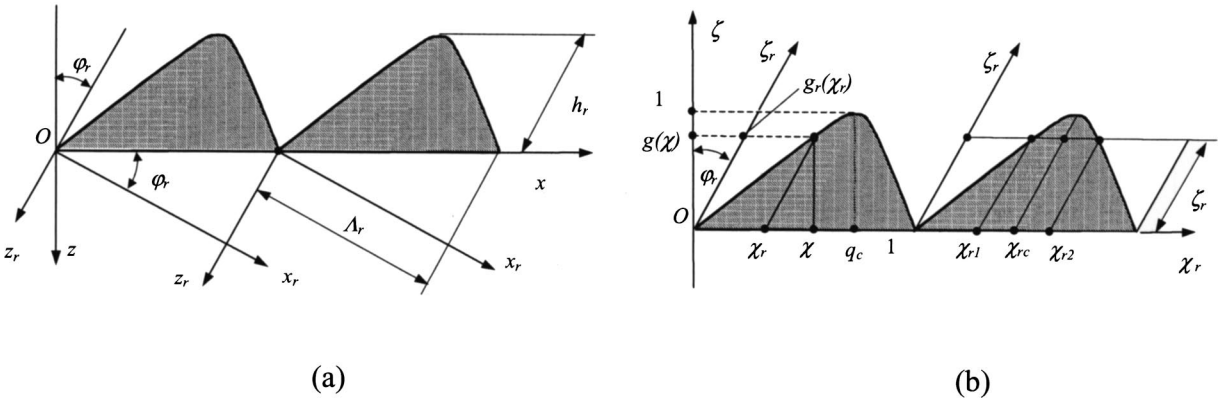

Fig. 2. Geometry and parameters for a surface-relief grating after coordinate rotation: (a) rotated coordinate system, (b) normalized rotated coordinate system and sublayers.

obtaining high diffraction efficiency. We restrict the groove shape to a unimodal single-blazed form, i.e., having a single peak and a single direction of blazing. The x axis is chosen perpendicular to the direction of grooves, the y axis is along the direction of grooves, and the z axis is perpendicular to the grating substrate, with its origin O at the bottom of the grating layer. The refractive-index distribution is periodic in the x-axis direction.

We now also introduce normalized coordinates χ, ζ that range from 0 to 1, within a single grating groove, as $\chi = x/\Lambda$, $\zeta = -z/h$. Figure 1(b) shows the normalized geometry and parameters. The groove profile $g(\cdot)$ in normalized coordinates is defined by $\zeta = g(\chi)$, where $0 \leqslant \chi \leqslant 1$, $0 \leqslant g(\chi) \leqslant 1$, and we denote the relative position of the groove's peak as $\chi = q_c$, so that $g(q_c) = 1$.

In dealing with slanted grooves, it is convenient to rotate the coordinate system[29–33] toward some slant direction. In our case, we rotated the coordinate system by an angle ϕ_r, as shown in Fig. 2. Figure 2(a) shows the geometry and the parameters in the rotated coordinate system. We introduce a rotated grating period Λ_r and a rotated maximum groove depth h_r as

$$\Lambda_r = \Lambda \cos \phi_r, \quad h_r = h/\cos \phi_r. \tag{1}$$

In this rotated coordinate system, the axis x_r is perpendicular to the slant direction, the axis y_r coincides with the axis y, and the axis z_r is along the slant direction. The origin of the rotated coordinate system is no longer the same for all grooves but shifts with period Λ along the x axis. Such shifting keeps the distribution of the refractive index periodic in the x_r-axis direction of the rotated coordinate system x_r, y_r, z_r.

Figure 2(b) shows the geometry and the parameters in the rotated normalized coordinate system χ_r, ζ_r, with

$$\chi_r = \frac{x_r/\cos \phi_r}{\Lambda}, \quad \zeta_r = -\frac{z_r}{h_r}. \tag{2}$$

The rotated groove profile is characterized by the function $\zeta_r = g_r(\chi_r)$, where $0 \leqslant \chi_r \leqslant 1$, $0 \leqslant g_\zeta(\chi_r) \leqslant 1$. Applying a coordinate rotation transformation from χ, ζ to χ_r, ζ_r, followed by simple algebraic manipulations, yields

$$g_r(\chi_r) = g(\chi), \quad \chi_r = \chi - pg(\chi), \tag{3}$$

with a new "slant parameter" p defined as

$$p = h \tan \phi_r/\Lambda. \tag{4}$$

The parameter $p\Lambda$ is essentially a projection of the rotated maximum groove depth h_r onto the coordinate axis χ, as found from Eq. (3) when $g = 1$ and $g = 0$ at a fixed value of the coordinate χ_r.

For unimodal groove profiles, we may characterize the rotated groove profile by its borders χ_{r1} and χ_{r2} at a certain groove depth level with normalized coordinate value ζ_r, so that $g_r(\chi_{r1,2}) = \zeta_r$, as depicted in Fig. 2(b). We also introduce the groove width $\Delta\chi_r = \chi_{r2} - \chi_{r1}$ and the groove central point $\chi_{rc} = (\chi_{r1} + \chi_{r2})/2$ at a certain ζ_r. For single-blazed gratings, with ζ_r that varies from 0 to 1, the

central points χ_{rc} have a trajectory along an oblique straight line oriented with angle ϕ_r, as depicted in Fig. 2(b).

To proceed, we now approximate the refractive-index distribution in each groove with a superposition of sinusoidal graded-refractive-index distributions, each of which has an arbitrary angular orientation ϕ_r, whose value must be optimized. Each sinusoidal distribution can be considered a "directionally averaged" grating with grating vector $\mathbf{K}_r$ oriented along axis x_r, with $|\mathbf{K}_r| = 2\pi/\Lambda_r$, as shown in Fig. 3. Accordingly, the surface-relief grating can now be characterized by a three-dimensional grating vector $\mathbf{K}_r$ rather than the usual two-dimensional grating vector. Mathematically, the approximation of the refractive-index distribution n can be written in the form of a finite complex Fourier series as

$$n^2 = \bar{n}^2 + \Delta n_M^2 \sum_{\Delta j} \bar{G}_{\Delta j} \exp(i \Delta j \mathbf{K}_r \mathbf{r}), \tag{5}$$

where n has period Λ with respect to the coordinate x and period 1 with respect to the normalized coordinate χ_r, $\mathbf{r} = (x_r, y_r, z_r)$, $\mathbf{K}_r \mathbf{r} = 2\pi\chi_r$, $i = \sqrt{-1}$, and $\Delta n_M^2 = n_M^2 - n_i^2$, with $\Delta j = 0, \pm 1, \pm 2, \ldots$. The essentially constant averaged refractive index $\bar{n}$ and averaged Fourier coefficients $\bar{G}_{\Delta j}$ can be determined by routine mathematical orthogonal least-squares approximation, yielding

$$\bar{n}^2 = \int_0^1 \int_0^1 n^2 \mathrm{d}\chi_r \mathrm{d}\zeta_r, \quad \bar{G}_{\Delta j} = \int_0^1 G_{\Delta j}(\zeta_r) \mathrm{d}\zeta_r, \tag{6}$$

with

$$G_{\Delta j}(\zeta_r) = \int_0^1 \frac{n^2 - \bar{n}^2}{\Delta n_M^2} \exp(-i 2\pi \Delta j \chi_r) \mathrm{d}\chi_r \tag{7}$$

and approximation error

$$\epsilon = \int_0^1 \int_0^1 n^4 \mathrm{d}\chi_r \mathrm{d}\zeta_r - \Delta n_M^4 \sum_{\Delta j} |\bar{G}_{\Delta j}|^2. \tag{8}$$

The averaged refractive index $\bar{n}$ and the averaged Fourier coefficients $\bar{G}_{\Delta j}$ are directly related to the groove profile $g(\chi)$ by integration, along the rotated ζ_r direction, with n having a value of either n_i or n_M:

$$\bar{n}^2 = n_i^2 + \Delta n_M^2 \bar{g}, \quad \bar{g} = \int_0^1 g(\chi) \mathrm{d}\chi, \tag{9}$$

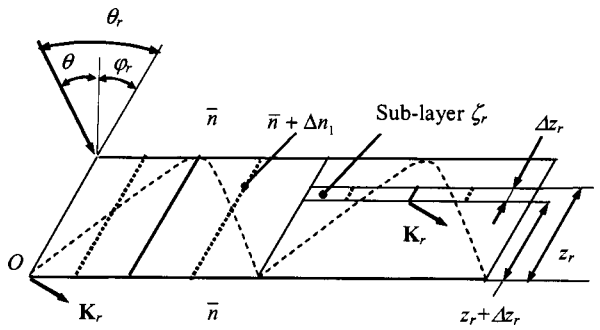

Fig. 3. Characterization of a surface-relief grating, both overall and in each layer, by sinusoidal graded-index gratings with a three-dimensional grating vector.

$$\bar{G}_{\Delta j} = \int_0^1 g_r(\chi_r) \exp(-i 2\pi \Delta j \chi_r) \mathrm{d}\chi_r, \quad \Delta j \neq 0, \tag{10}$$

where $\bar{G}_0 = 0$. We note that, in accordance with Eqs. (3), (4), and (10), the averaged Fourier coefficients $\bar{G}_{\Delta j}$ ($\Delta j \neq 0$) depend on ϕ_r while the averaged refractive index $\bar{n}$ does not. Moreover, the directionally averaged sinusoidal graded-index grating with period $\Lambda_r/\Delta j$ can be characterized with the averaged Fourier coefficients $\bar{G}_{\Delta j}$ and their complex conjugates $\bar{G}^*_{\Delta j}$ and also by a refractive-index modulation term $\Delta n_{\Delta j}$. Such a $\Delta n_{\Delta j}$ can be obtained by comparing Eq. (5) with that obtained for sinusoidal graded-index gratings,[27] which yields $\Delta n_{\Delta j} = \Delta n_M^2 |\bar{G}_{\Delta j}| / \bar{n}$.

We now treat the directionally averaged gratings as embedded inside a medium with an averaged refractive index $\bar{n}$ (see Fig. 3). Thus the incidence angle θ_{inc} must be replaced by an incidence angle θ in accordance with Snell's law, i.e., $n_i \sin\theta_{\mathrm{inc}} = \bar{n} \sin\theta$. Accordingly, the Bragg incidence angle for the jth diffraction order, denoted as $\theta_{\mathrm{inc},j}$, must be replaced by θ_j, where $n_i \sin\theta_{\mathrm{inc},j} = \bar{n} \sin\theta_j$. In the rotated coordinate system, we denote the incidence angle as $\theta_r = \theta + \phi_r$ and the Bragg incidence angle as θ_{rj}. The Bragg condition in the rotated coordinate system is

$$\sin\theta_{rj} = j \frac{\lambda}{2\bar{n}\Lambda_r}, \qquad \theta_{rj} = \theta_j + \phi_r. \tag{11}$$

Solving Eqs. (11) with slant parameter p [see Eq. (4)] yields the Bragg incidence angle θ_j in the nonrotated coordinate system:

$$\bar{n} \sin\theta_j = \frac{j\lambda}{2\Lambda} - \frac{\Lambda p}{h} \left[\frac{\bar{n}^2}{1 + (\Lambda p/h)^2} - \left(\frac{j\lambda}{2\Lambda} \right)^2 \right]^{1/2}. \tag{12}$$

Diffraction orders inside the grooves of the directionally averaged gratings have propagation vectors[27,28]

$$\boldsymbol{\sigma}_j = \boldsymbol{\sigma}_0 - j\mathbf{K}_r, \qquad \boldsymbol{\sigma}_j = k\bar{n}(s_{jr}, 0, c_{0r}), \tag{13}$$

where $k = 2\pi/\lambda$ and, for mathematical convenience, we defined parameters

$$s_{jr} = \sin\theta_r - j 2 \sin\theta_{rj}, \qquad c_{0r} = \cos\theta_r = (1 - s_{0r}^2)^{1/2}. \tag{14}$$

B. Two-Wave Bragg Diffraction in Surface-Relief Gratings

Effective refractive-index theory[2,3] is exploited for analyzing subwavelength surface-relief gratings where only the zero diffraction order exists. We now develop an effective grating theory in order to obtain an effective grating model for analyzing resonance domain surface-relief gratings where, in addition to the zero order, a nonevanescent first diffraction order also exists, i.e., two-wave diffraction. For such resonance domain gratings, the ratio Λ/λ of grating period to wavelength must exceed a subwavelength bound $\Lambda_{\mathrm{subw}}/\lambda$,[2,3] which, in our case, is

$$\Lambda/\lambda > \Lambda_{subw}/\lambda = (\bar{n} + \bar{n}\sin\theta_1)^{-1}, \tag{15}$$

where θ_1 is the first Bragg incidence angle in the medium with averaged refractive index $\bar{n}$. The two-wave criterion of the Bragg diffraction regime,[34] where the total power ε_{high} of all diffraction orders, other than the zero and first orders, can be neglected, is

$$\rho^{-2} \leqslant \varepsilon_{high}, \tag{16}$$

with

$$\rho = \left(\frac{\lambda}{\Lambda_r}\right)^2 \bar{n}\Delta n_1, \qquad \rho^{-2} = \left(\frac{\Lambda}{\lambda}\right)^4 (\bar{n}\Delta n_1)^2 \cos^4\phi_r. \tag{17}$$

Accordingly, the subwavelength bound of relation (15) and the two-wave criterion of Eqs. (16) and (17) restrict the period Λ to the interval ranging from Λ_{subw} up to $\Lambda_{two\ wave}$, where $\Lambda_{two\ wave}$ is the period for which $\rho^{-2} = \epsilon_{high}$. For typical optical materials, this interval is comparable with λ, so that the two-wave Bragg diffraction regime basically occurs in the resonance domain of diffraction. It should be noted that the two-wave Bragg diffraction criterion in Eqs. (17) is independent of grating thickness. Thus the two-wave Bragg diffraction occurs when we consider gratings formed either with complete grooves or with individual sublayers of grooves.

To relate the diffracted orders of the original resonance domain surface-relief gratings to those of directionally averaged graded-index gratings, we treat each groove in the surface-relief grating as a continuum of infinitesimal sublayers of thickness Δz_r, each located at a different normalized coordinate value ζ_r. The sublayer therefore extends from the upper surface z_r to the lower surface $z_r + \Delta z_r$ in rotated direction z_r and is bounded by two oblique parallel straight lines oriented at angle ϕ_r at the left and right edges of the groove, as shown in Fig. 3. In each of these sublayers, in rotated coordinates x_r, y_r, z_r, the refractive index n can be expanded in a Fourier series and the electric field $\mathbf{E}$ can be expanded in a series of coupled waves corresponding to diffraction orders. These expansions are then incorporated into the generalized Helmholtz equation to form coupled-wave equations with a "sublayer matrix" of coefficients $\mathbf{M}(\zeta_r)$. The coupled-wave equations are solved to obtain the complex amplitudes $S_0(z_r+\Delta z_r;\zeta_r)$ of the zero diffraction order and $S_1(z_r+\Delta z_r;\zeta_r)$ of the first diffraction order at the exit (lower surface in Fig. 3) of each sublayer. The derivation presented in Appendix A leads to a "transmittance matrix" $\mathbf{T}(\zeta_r;\Delta z_r)$ that describes the transformation of the complex amplitudes $S_0(z_r;\zeta_r)$ and $S_1(z_r;\zeta_r)$ at the entrance (upper surface in Fig. 3) of each sublayer to those at the exit. This matrix is written [from Eq. (A9) in Appendix A] as

$$\mathbf{T}(\zeta_r;\Delta z_r) = \exp[ik\bar{n}\mathbf{M}(\zeta_r)\Delta z_r]. \tag{18}$$

To represent the surface-relief grating by an effective grating whose refractive index varies in the x_r direction but not in the z_r direction (just like volume gratings), it is necessary that all sublayers have the same characteristics in terms of light propagation. This implies that the eigenvectors of matrix $\mathbf{T}(\zeta_r;\Delta z_r)$ and accordingly those of $\mathbf{M}(\zeta_r)$ should be the same for all sublayers. Thus the matrices $\mathbf{M}(\zeta_r)$ of all sublayers should commute. Therefore the sublayer matrices $\mathbf{M}(\zeta_{r1})$ and $\mathbf{M}(\zeta_{r2})$ of any two sublayers should commute, and their commutator $\mathbf{Q}_{12} = \mathbf{M}(\zeta_{r1})\mathbf{M}(\zeta_{r2}) - \mathbf{M}(\zeta_{r2})\mathbf{M}(\zeta_{r1})$ should be zero for any ζ_{r1} and ζ_{r2}.

To proceed, we substitute the sublayer matrices $\mathbf{M}(\zeta_{r1})$ and $\mathbf{M}(\zeta_{r2})$, defined in Appendix A [Eq. (A7)], into $\mathbf{Q}_{12}$ to yield a 2×2 matrix in the two-wave Bragg diffraction regime:

$$\mathbf{Q}_{12} = \mathbf{Q}_{12slant} + \vartheta_1 \mathbf{Q}_{12Bragg}, \tag{19}$$

with

$$\mathbf{Q}_{12slant} = c_{0r}^{-2}[\kappa_{01}(\zeta_{r1})\kappa_{01}^{*}(\zeta_{r2}) - \kappa_{01}^{*}(\zeta_{r1})\kappa_{01}(\zeta_{r2})]\begin{bmatrix} 1 & 0 \\ 0 & -1 \end{bmatrix}, \tag{20}$$

$$\mathbf{Q}_{12Bragg} = c_{0r}^{-2}\begin{bmatrix} 0 & \Delta\kappa_{01} \\ \Delta\kappa_{01}^{*} & 0 \end{bmatrix}, \qquad \Delta\kappa_{01} = \kappa_{01}(\zeta_{r1}) - \kappa_{01}(\zeta_{r2}), \tag{21}$$

$$\vartheta_1 = \frac{1}{2}(1 - s_{1r}^2 - c_{0r}^2), \tag{22}$$

and s_{jr}, c_{0r} given in Eqs. (14). Coefficient $\kappa_{01}(\zeta_r)$ is proportional to Fourier coefficient $G_1(\zeta_r)$, as defined [Eqs. (A8)] in Appendix A.

To obtain $\mathbf{Q}_{12}=0$, it is best that both terms of Eq. (19) be zero, i.e., $\mathbf{Q}_{12slant}=0$ and $\vartheta_1\,\mathbf{Q}_{12Bragg}=0$. The term $\vartheta_1\,\mathbf{Q}_{12Bragg}$ becomes zero when the incidence angle is close to the Bragg incidence angle θ_1 [Eq. (12)], for which $\vartheta_1=0$. The term $\mathbf{Q}_{12slant}$ becomes zero by properly choosing the angular orientation ϕ_r, namely, ϕ_s. Specifically, $\mathbf{Q}_{12slant}$ becomes zero when the phase of either $\kappa_{01}(\zeta_r)$ [Eqs. (A8)] or, equivalently, $G_1(\zeta_r)$ [Eq. (A2)] does not depend on sublayer coordinate ζ_r. For unimodal single-blazed gratings, such phase independence occurs when all central points χ_{rc} of the sublayers lie along a line with angular orientation ϕ_s, which follows from Eqs. (A2) and (A3) of Appendix A. Also, the phase independence implies that the Fourier coefficients $G_1(\zeta_r)$ at different ζ_r are matched in phase, so the modulus $|\bar{G}_1|$ of their sum, $\bar{G}_1 = G_{1s}$ [Eq. (6)], is maximized while the corresponding approximation error ϵ [Eq. (8)] is accordingly minimized. The refractive-index value modulation term Δn_1, which is proportional to $|\bar{G}_1|$, also reaches its maximum value of Δn_s at ϕ_s.

The transmittance matrix $\bar{\mathbf{T}}$ of the overall surface-relief grating is a product of all the transmittance matrices $\mathbf{T}(\zeta_r;\Delta z_r)$ of each sublayer, embedded in the same medium with refractive index $\bar{n}$. When the eigenvectors for all the sublayer matrices $\mathbf{M}(\zeta_r)$ are the same, i.e., when $\mathbf{Q}_{12}=0$, then one need not multiply matrices $\mathbf{T}(\zeta_r;\Delta z_r)$ [Eq. (18)] but simply add matrices $\mathbf{M}(\zeta_r)$. Specifically, we obtain $\bar{\mathbf{T}}$ with "averaged grating matrix" $\bar{\mathbf{M}}$ as

$$\bar{\mathbf{T}} = \exp(ik\bar{n}\bar{\mathbf{M}}h_r), \qquad \bar{\mathbf{M}} = \int_0^1 \mathbf{M}(\zeta_r)\mathrm{d}\zeta_r, \tag{23}$$

where the elements of the averaged grating matrix $\bar{\mathbf{M}}$ are found from

$$\bar{M}_{j,j'} = c_{0r}^{-1}(\bar{\kappa}_{j,j'} + \vartheta_j\delta_{j'-j}), \tag{24}$$

where

$$\bar{\kappa}_{j,j'} = \delta n_M^2 \mathbf{e}_j \cdot \mathbf{e}_{j'}\bar{G}_{j'-j}, \qquad \delta n_M^2 = \Delta n_M^2/2\bar{n}^2, \tag{25}$$

with $\vartheta_0=0$, ϑ_1 and $\bar{G}_{j'-j}$ given in Eqs. (22) and (10), respectively, $j,j'=0$ or 1, and $\mathbf{e}_j$ denoting the unit polarization vector in diffraction order j. The overall results lead to a single overall directionally averaged grating (with a particular rotation angle ϕ_s and averaged matrix $\bar{\mathbf{M}}$ of coupled-wave equations), namely, an "effective grating" for the original surface-relief grating.

3. CALCULATION OF DIFFRACTION EFFICIENCY BY MEANS OF THE EFFECTIVE GRATING MODEL

We see now that by properly choosing the rotation angle as ϕ_s and at a nearly Bragg incidence angle, one can indeed obtain the commuting property $\mathbf{Q}_{12}=0$ between sublayers and, after averaging, an averaged overall grating matrix $\bar{\mathbf{M}}$ for the effective grating. Thus the diffraction efficiency and the phase of the zero and first diffraction orders for the effective grating with $\bar{\mathbf{M}}$ are essentially the same as those for the original surface-relief grating, within the bounds of our model. The Bragg incidence angle $\theta_1|_{p=p_s}$ for the effective grating is obtained from Eq. (12) at $j=+1$ and $p=p_s$, with

$$p_s = \frac{h\tan\varphi_s}{\Lambda}, \tag{26}$$

which maximizes $|\bar{G}_1|$ [Eqs. (3) and (10)].

As is evident from Eq. (12), the Bragg incidence angle for gratings with slanted (also sawtooth) groove profiles differs from that with symmetrical groove profiles. This explains why the first-order diffraction efficiency was only 51% rather than approximately 100% for a 30° incidence angle[14] for the case of a sawtooth grating with $\Lambda/\lambda=1$.

The complex amplitudes $S_1(z_r), S_0(z_r)$ of the diffraction orders of the effective grating can be readily obtained by resorting to the relatively simple theory for sinusoidal graded-index gratings in the two-wave Bragg regime[27] with averaged grating matrix $\bar{\mathbf{M}}$. Specifically, the differential equation $\mathbf{S}'(z_r)=ik\bar{n}\bar{\mathbf{M}}\mathbf{S}(z_r)$ for $\mathbf{S}=(S_0,S_1)$, combined with Eqs. (23) and (24) and the first-order boundary conditions[27,28] $S_0(-h_r)=1$ and $S_1(-h_r)=0$, yields closed-form analytic solutions for the complex amplitudes of the zero and first diffraction orders:

$$S_0^{(\mathrm{out})} = \exp(i\xi)(\cos\mu - i\xi\sin\mu/\mu), \tag{27}$$

$$S_1^{(\mathrm{out})} = i\exp(i\xi)\nu\sin\mu/\mu, \tag{28}$$

where

$$\mu = (\nu^2+\xi^2)^{1/2}, \tag{29}$$

$$\nu = h_s k\bar{n}\frac{\bar{\kappa}_{01}}{c_{0r}}, \qquad \xi = h_s k\bar{n}\frac{\vartheta_1}{2c_{0r}}, \tag{30}$$

with $h_s=h/\cos\phi_s$ and $\phi_r=\phi_s$.

In our model, we matched the coordinate system to the groove slant direction ϕ_s of the effective grating. Thus the diffraction efficiencies of the zero and first orders are just $\eta_0=|S_0^{(\mathrm{out})}|^2$ and $\eta_1=|S_1^{(\mathrm{out})}|^2$, respectively, with corresponding phases $\arg S_0^{(\mathrm{out})}$ and $\arg S_1^{(\mathrm{out})}$, which may be derived from Eqs. (27) and (28), respectively. At the Bragg incidence angle, the first-order Bragg efficiency $\eta_1=\eta_{\mathrm{Bragg}}$ is

$$\eta_{\mathrm{Bragg}} = \sin^2\nu_{\mathrm{Bragg}}, \tag{31}$$

where

$$\nu_{\mathrm{Bragg}} = 2\pi\frac{h}{\lambda}\frac{\bar{n}\bar{\kappa}_{01}}{\cos\phi_s c_{0s\mathrm{Bragg}}} \tag{32}$$

with θ_{s1} and $c_{0s\mathrm{Bragg}}$, from Eqs. (11) and (14), given by

$$c_{0s\mathrm{Bragg}} = (1-\sin^2\theta_{s1})^{1/2}, \qquad \sin\theta_{s1} = \frac{\lambda}{2\bar{n}\Lambda\cos\phi_s}. \tag{33}$$

The parameter $\bar{\kappa}_{01}$ differs in the cases of TE and TM polarizations:

$$\bar{\kappa}_{01\mathrm{TE}} = \delta n_M^2 G_{1s}, \qquad \bar{\kappa}_{01\mathrm{TM}} = \bar{\kappa}_{01\mathrm{TE}}(1-2\sin^2\theta_{s1}). \tag{34}$$

Using Eqs. (10), (31), (32), and (34), we can conclude that surface-relief gratings with different groove profiles but equal first averaged Fourier coefficient G_{1s} will all have the same Bragg efficiency. This conclusion is in agreement with the empirical criterion of the "equivalence rule" for surface-relief gratings.[22,35]

To proceed, we now derive the needed parameters of the surface-relief gratings that would provide the required diffraction efficiencies. Since the functions $c_{0r\mathrm{Bragg}}$ and $\bar{\kappa}_{01}$ depend only on Λ/λ and ϕ_s, we need to solve Eqs. (31) and (32) in order to determine the groove depth h that would lead to the desired Bragg efficiency η_{Bragg} at the Bragg incidence angle. For a specific value of η_{Bragg}, there are two main solutions for the optimal groove depths, which differ in the cases of TE and TM polarizations. They are

$$\frac{h}{\lambda} = \frac{c_{0s\mathrm{Bragg}}\cos\phi_s}{2\pi\bar{n}\bar{\kappa}_{01}}\left[\frac{\pi}{2} \pm \left(\frac{\pi}{2} - \arcsin\sqrt{\eta_{\mathrm{Bragg}}}\right)\right]. \tag{35}$$

It should be noted that Eqs. (31) and (32) differ from those used in scalar diffraction theory.[36] They analytically show how the diffraction efficiency is reduced when the groove depth deviates from the optimal value of Eq. (35).

To choose the parameters of the groove profile so as to achieve a required value of Bragg incidence angle $\theta_1=\theta_{\mathrm{req}}$ for a given grating period Λ and a desired Bragg efficiency η_{Bragg}, we used Eq. (33) with $\theta_{r1}=\theta_{\mathrm{req}}+\phi_s$. Specifically, after some algebraic manipulations, we obtain the optimal groove slant angle θ_s as

$$\tan \phi_s = \frac{\bar{n}\Lambda}{\lambda}\left\{\cos \theta_{\mathrm{req}} - \left[1 - \left(\sin \theta_{\mathrm{req}} - \frac{\lambda}{\bar{n}\Lambda}\right)^2\right]^{1/2}\right\}. \tag{36}$$

Then, substituting the ϕ_s from Eq. (36) into Eqs. (26) and (35), we find the corresponding optimal groove depth and slant parameter p_s. Finally, using Eqs. (3), (4), (26), and (A3) with $g(q_c)=1$, we relate the optimal slant parameter p_s to relative groove peak position q_c:

$$q_c = 0.5 + p_s. \tag{37}$$

Any small deviation of the incidence angle from the Bragg incidence angle $\theta_1|_{p=p_s}$ leads to a small reduction of efficiency η_1 from the Bragg efficiency η_{Bragg} down to $\eta_{\mathrm{mis}}\eta_{\mathrm{Bragg}}$. The relative reduction factor η_{mis} is derived from Eq. (28) as

$$\eta_{\mathrm{mis}} = \frac{\sin^2[(\nu^2+\xi^2)^{1/2}]}{\sin^2 \nu}\left(1+\frac{\xi^2}{\nu^2}\right)^{-1}, \tag{38}$$

with ξ and ν defined in Eqs. (30). For example, with $\eta_{\mathrm{Bragg}}=1.0$ and $\eta_{\mathrm{mis}}=0.9$, Eq. (38) yields $\xi_{\mathrm{mis}}=0.507$. The corresponding boundary incidence angles $\theta_1^{\pm}$ (in a medium with averaged refractive index $\bar{n}$) and angular selectivity $\Delta\theta_1=\theta_1^+-\theta_1^-$ are analytically derived by using Eqs. (14), (22), (30), (32), and (38), with $\nu=\nu_{\mathrm{Bragg}}$, yielding

$$\sin \theta_1^{\pm} = F^{\pm} - (\tan \phi_s)[\cos^2 \phi_s - (F^{\pm})^2]^{1/2}, \tag{39}$$

where

$$F^{\pm} = \frac{\lambda}{2\bar{n}\Lambda} \pm \frac{\xi_{\mathrm{mis}} \cos^3 \phi_s}{\pi}\frac{\Lambda}{h}c_{0s\mathrm{Bragg}}. \tag{40}$$

Now, besides the effective grating with ϕ_s, p_s, and maximized Δn_s, the surface-relief grating also includes additional directionally averaged gratings, with different ϕ_r, $p=p_s+\Delta p$, and lower Δn_1. In general, it is necessary to consider only those additional gratings that have relatively high Δn_1; in particular, only those with $\Delta n_1/\Delta n_s \geqslant \delta_{\mathrm{low}}$, where δ_{low} is a fixed small threshold value. In other words, we consider only additional gratings with p between boundaries p_{low}^- and p_{low}^+ defined by equations $p_{\mathrm{low}}^{\pm}=p_s\pm\Delta p_{\mathrm{low}}$ and $\Delta n_1/\Delta n_s|_{p=p_{\mathrm{low}}^{\pm}}=\delta_{\mathrm{low}}$. All these parameters are depicted in Fig. 4, which shows $\Delta n_1/\Delta n_s$ as a function of Δp for a continuous range of directionally averaged gratings. Some of the light from each additional directionally averaged grating will be diffracted into the −1st instead of the +1st order of the original surface-relief grating, as evident from Eq. (12) with $j=-1$. To ensure that this undesirable diffracted light is minimal, the nearest −1st Bragg incidence angle $\theta_{-1,\mathrm{low}}=\theta_{-1}|_{p=p_{\mathrm{low}}^-}$ of the additional grating with $p=p_{\mathrm{low}}^-$ must be sufficiently different from the +1st Bragg incidence angle $\theta_1|_{p=p_s}$ of the effective grating. In particular, we demand that $\theta_{-1,\mathrm{low}}$ should be further away from $\theta_1|_{p=p_s}$ than the boundary incidence angle θ_1^- of Eq. (39) when $\eta_{\mathrm{mis}}=0.9$. In the worst case,

$$\theta_{-1,\mathrm{low}} = \theta_1^-. \tag{41}$$

For a given groove depth h, the ratio Λ/λ is constrained to be smaller than an upper bound value $\Lambda_{\mathrm{up}}/\lambda$ found by using Eqs. (12), (39), and (41) when $j=-1$ and $p=p_{\mathrm{low}}^-$. Such a constraint provides the range for applicability of our effective grating model.

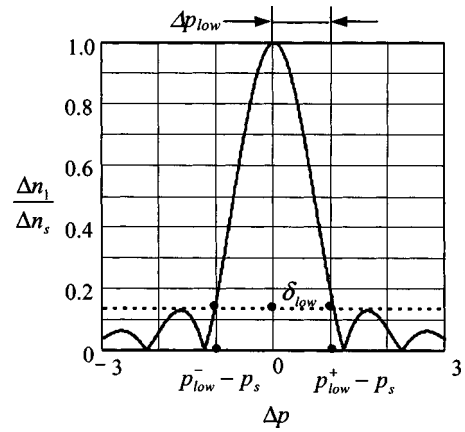

Fig. 4. Relative refractive-index modulation term $\Delta n_1/\Delta n_s$ as a function of groove deviation Δp from the slant of the effective grating. For the effective grating $\Delta n_1=\Delta n_s$, δ_{low} is the threshold value, $2\Delta p_{\mathrm{low}}$ the bandwidth, and p_{low}^- and p_{low}^+ the boundaries.

To conclude, we found several limits and bounds for the applicability of effective grating theory. They include the following: (1) The groove profile should be unimodal and single blazed, (2) the period Λ must be greater than Λ_{subw} in order to satisfy the subwavelength structure bound [relation (15)], (3) the value of $\rho^{-2}=\epsilon_{\mathrm{high}}$ must be much smaller than 1 in order to satisfy the two-wave criterion, and (4) the period Λ must be less than Λ_{up} in order to reduce the influence of additional directionally averaged gratings related to Eq. (41). Another restriction, now quantitatively expressed as $|\bar{\kappa}_{01}/c_{0s\mathrm{Bragg}}| \ll 1$, with $\bar{\kappa}_{01}$ and $c_{0s\mathrm{Bragg}}$ defined in Eqs. (33) and (34), arises from the justification for neglecting the second-order derivatives in Eq. (A6).

4. DIFFRACTION EFFICIENCY FOR REPRESENTATIVE GRATING GROOVE PROFILES

We consider two representative examples of surface-relief grating groove profiles. One is a triangular groove profile and the other a slanted sinusoidal groove profile, both of which are characterized by a relative groove peak position q_c within the groove. A value $q_c=0.5$ ($p_s=0$) denotes a symmetrical groove profile, whereas $q_c=1.0$ ($p_s=0.5$) denotes a blazed groove profile with one vertical edge. The value of $q_c>1.0$ ($p_s>0.5$) denotes an "overhanging groove" profile. All these profiles are unimodal and single blazed.

The triangular groove profile is formed with two straight lines and can be written as

$$g(\chi) = \begin{cases} \chi/q_c, & 0 \leqslant \chi \leqslant q_c \\ (1-\chi)/(1-q_c), & q_c \leqslant \chi \leqslant 1 \end{cases}. \tag{42}$$

Substituting Eq. (42) into Eqs. (10) and (A2) yields, after integration, the closed-form analytical expressions for the Fourier coefficients $\bar{G}_{\Delta j}$ and $G_{\Delta j}(\zeta_r)$:

$$\bar{G}_{\Delta j} = \frac{2\exp(i\Delta\alpha)}{(\pi\Delta j)^2(4\Delta p^2 - 1)} \begin{cases} -i\sin(\Delta\alpha) & \text{when } \Delta j = 2,4,\ldots \\ \cos(\Delta\alpha) & \text{when } \Delta j = 1,3,\ldots \end{cases}, \tag{43}$$

$$G_{\Delta j}(\zeta_r) = -\zeta_r \operatorname{sinc}(\Delta j\zeta_r)\exp(i2\Delta\alpha\zeta_r) + 0.5\delta_{\Delta j}, \tag{44}$$

with $\Delta\alpha = \pi\Delta j\Delta p$, $\bar{G}_0 = 0$, and $|G_{1s}| = 2/\pi^2$ occurring at $\Delta p = 0$, where $\Delta p = p - p_s$.

The slanted sinusoidal groove profile formed by rotation of a symmetrical sinusoidal groove profile $g_{\text{sym}}(\chi_{\text{sym}}) = 0.5[1 - \cos(2\pi\chi_{\text{sym}})]$ can be written in parametric form, similar to Eq. (3), as

$$g(\chi) = g_{\text{sym}}(\chi_{\text{sym}}), \qquad \chi = \chi_{\text{sym}} + (q_c - 0.5)g_{\text{sym}}(\chi_{\text{sym}}), \tag{45}$$

with $0 \leqslant \chi_{\text{sym}} \leqslant 1$. Substituting Eq. (45) into Eqs. (10) and (A2) yields, after integration, the closed-form analytical expressions for the Fourier coefficients $\bar{G}_{\Delta j}$ and $G_{\Delta j}(\zeta_r)$:

$$\bar{G}_{\Delta j} = -\frac{J_{\Delta j}(\Delta\alpha)}{2\Delta\alpha} i\exp(i\Delta\alpha - i\pi\Delta j/2), \tag{46}$$

$$G_{\Delta j}(\zeta_r) = -\alpha_r \operatorname{sinc}(\Delta j\alpha_r)\exp(i2\Delta\alpha\zeta_r) + 0.5\delta_{\Delta j}, \tag{47}$$

with $\alpha_r = 2\arcsin\sqrt{\zeta_r}/\pi$, $\Delta\alpha = \pi\Delta j\Delta p$, $\bar{G}_0 = 0$, and $|G_{1s}| = 0.25$ occurring at $\Delta p = 0$, where $\Delta p = p - p_s$.

For the triangular slanted as well as the sinusoidal groove profiles, the behavior of $|G_1|$, and consequently of $\Delta n_1 = \Delta n_M^2|\bar{G}_1|/\bar{n}$, as a function of Δp, is similar to that shown in Fig. 4, where there is one central lobe and several sidelobes. It is reasonable to choose the value of δ_{low} as the height of the first sidelobe peak. Then using $\Delta n_1/\Delta n_s|_{\Delta p = \Delta p_{\text{low}}} = \delta_{\text{low}}$, we find that $\Delta p_{\text{low}} = 1.3524$ for the triangular groove profile and $\Delta p_{\text{low}} = 1.052$ for the sinusoidal groove profile. Also, for both profiles, substituting Eqs. (42) and (45) into Eq. (9) yields $\bar{g} = 0.5$ and $\bar{n} = [(n_M^2 + n_i^2)/2]^{1/2}$.

With our effective grating model, we calculated the Bragg diffraction efficiencies as a function of certain groove parameters by using Eqs. (31)–(34). Representative results are shown in Figs. 5–7. Figure 5 shows the Bragg diffraction efficiency of the +1st and zero diffraction orders as a function of the groove aspect ratio, depth/period (h/Λ), for surface-relief gratings with symmetrical ($q_c = 0.5$) triangular groove profiles, as denoted by the bold curves. The Bragg incidence angle was $\theta_{\text{inc},1} = 30°$, $\lambda/\Lambda = 1.0$, the refractive index of the groove material was $n_M = \sqrt{2.5}$, and TE polarization was used. For comparison, we also show the results obtained numerically by RCWA,[14] as denoted by the thin curves. As evident, there is close agreement between the results.

Figure 6 shows the Bragg diffraction efficiency of the +1st diffraction order as a function of h/Λ for surface-relief gratings with symmetrical triangular as well as sinusoidal groove profiles, denoted by the bold curves. The Bragg incidence angle was $\theta_{\text{inc},1} = 45°$, $\lambda/\Lambda = 1.414$, the refractive index of the groove material was $n_M = 1.66$, and TE polarization was used. Again, for comparison we show the results obtained numerically by RCWA,[16] as denoted by the thin curves. As evident, there is close agreement between the results.

Figure 7 shows, in both TE and TM polarizations, the Bragg diffraction efficiency of the +1st diffraction order as a function of λ/Λ for deep ($h/\Lambda = 2.0$) surface-relief gratings with symmetrical sinusoidal groove profiles, as denoted by the bold curves. The Bragg incidence angle $\theta_{\text{inc},1}$ was set at each λ/Λ, and the refractive index of the groove material was $n_M = 1.66$. Again, for comparison we show the results obtained numerically by RCWA,[16] as denoted

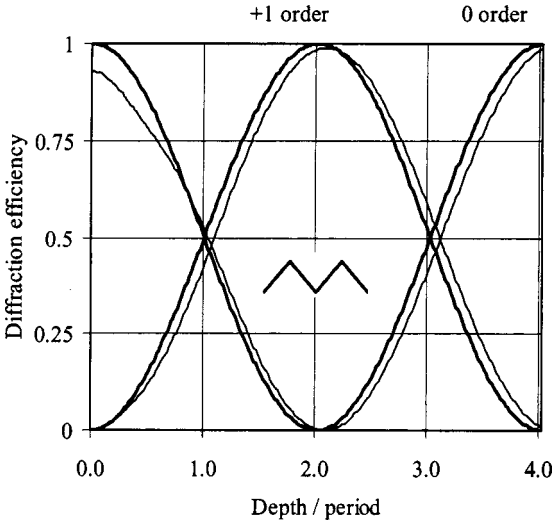

Fig. 5. Bragg diffraction efficiency as a function of aspect ratio h/Λ, for a surface relief grating with symmetrical ($q_c = 0.5$) triangular groove profile. The Bragg incidence angle was $\theta_{\text{inc},1} = 30°$, $\lambda/\Lambda = 1.0$, refractive index of grooves $n_M = \sqrt{2.5}$, and TE polarization. Bold curves, effective grating model; thin curves, numerical RCWA.[14]

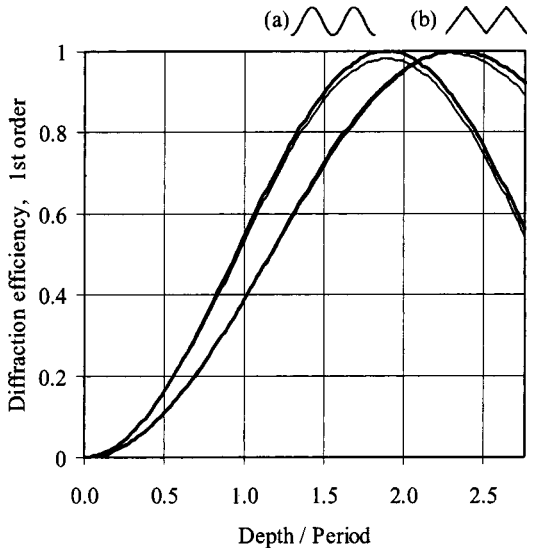

Fig. 6. Bragg diffraction efficiency of the +1st order as a function of aspect ratio h/Λ, for a surface relief grating with symmetrical ($q_c = 0.5$) groove profile: (a) sinusoidal, (b) triangular. The Bragg incidence angle was $\theta_{\text{inc},1} = 45°$, $\lambda/\Lambda = 1.414$, refractive-index of grooves $n_M = 1.66$, and TE polarization. Bold curves, effective grating model; thin curves, numerical RCWA.[16]

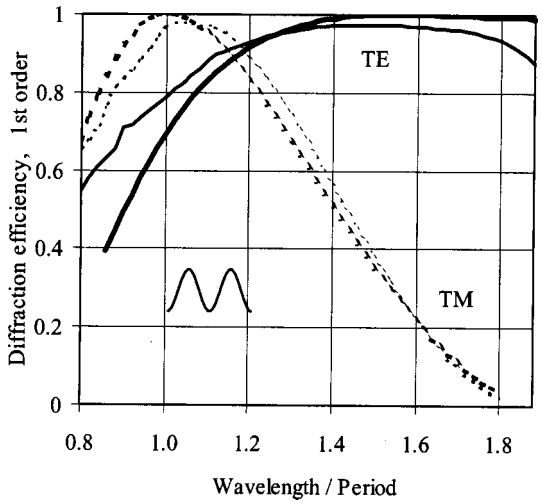

Fig. 7. Bragg diffraction efficiency of the +1st order as a function of ratio λ/Λ for a surface-relief grating with symmetrical ($q_c=0.5$) sinusoidal groove profile. The Bragg incidence angle $\theta_{\text{inc},1}$ was set at each λ/Λ, $h/\Lambda=2.0$; refractive index of grooves $n_M=1.66$. Bold curves, effective grating model; thin curves, numerical RCWA.[16]

by the thin curves. As evident, for both the TE and TM polarizations there is close agreement between the results.

Finally, we calculated the diffraction efficiency of the +1st diffraction order as a function of the incidence angle θ_{inc} for deep surface-relief gratings with symmetrical sinusoidal groove profiles. The Bragg incidence angle was $\theta_{\text{inc},1}=45°$, $\lambda/\Lambda=1.414$, the refractive index of the groove material was $n_M=1.66$, and TE polarization was used. The aspect ratio was chosen as $h/\Lambda=1.9$ for maximizing the Bragg diffraction efficiency. The agreement for diffraction efficiency values was within 3% over incidence angles ranging from 34° to 54°.

5. CHOICE OF GRATING PARAMETERS FOR HIGH DIFFRACTION EFFICIENCY

To determine the optimal groove depth and grating period that would result in high diffraction efficiency for the surface-relief gratings, we used Eqs. (35) and (41). Specifically, we calculated the optimal aspect ratio h/Λ as a closed-form analytical function of the normalized grating period Λ/λ at different Bragg diffraction efficiencies η_{Bragg} [Eq. (35)] and found the boundaries beyond which it is not possible to obtain high diffraction efficiency for the surface-relief gratings [Eq. (41)]. The results are presented in Figs. 8 and 9. Figure 8 shows optimal h/Λ as a function of Λ/λ, at different high Bragg diffraction efficiencies and TE and TM polarizations, for surface-relief gratings with triangular sawtooth groove profiles ($q_c=1$) and a groove material refractive index $n_M=1.46$. Figure 9 shows optimal h/Λ as a function of Λ/λ, at different high Bragg diffraction efficiencies and TE and TM polarizations, for surface-relief gratings with sinusoidal slanted groove profiles ($\phi_s=17°$) and groove material refractive index $n_M=1.66$. In both Figs. 8 and 9, the Bragg incidence angle $\theta_{\text{inc},1}$ was set at each Λ/λ. Also depicted in Figs. 8 and 9 is the two-wave criterion of the Bragg diffraction regime, ρ^{-2} [Eq. (17)], as a function of Λ/λ.

As evident in Figs. 8 and 9, the aspect ratio h/Λ must be higher with TM polarization than with TE polarization in order to achieve the same Bragg diffraction efficiencies. Also, for each polarization there are two ranges, where for a specific normalized grating period Λ/λ, two different as-

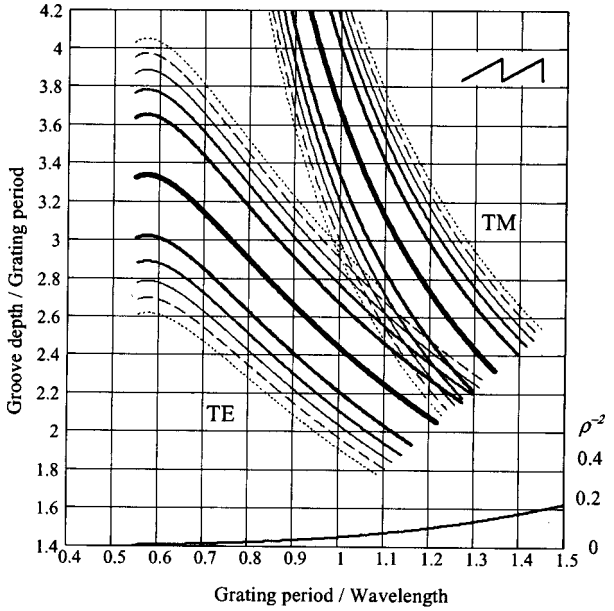

Fig. 8. Optimal aspect ratio h/Λ as a function of Λ/λ and their boundaries for obtaining high Bragg diffraction efficiency η_{Bragg} for a surface-relief grating with triangular sawtooth groove profile ($q_c=1$). Refractive index of grooves $n_M=1.46$. ρ^{-2} is a two-wave criterion of the Bragg diffraction regime with $\eta_{\text{Bragg}}=100\%$ in TE polarization. From bold to thin curves: $\eta_{\text{Bragg}}=100\%$, 98%, 96%, 94%; dashed curves, 92%, dotted curves, 90%.

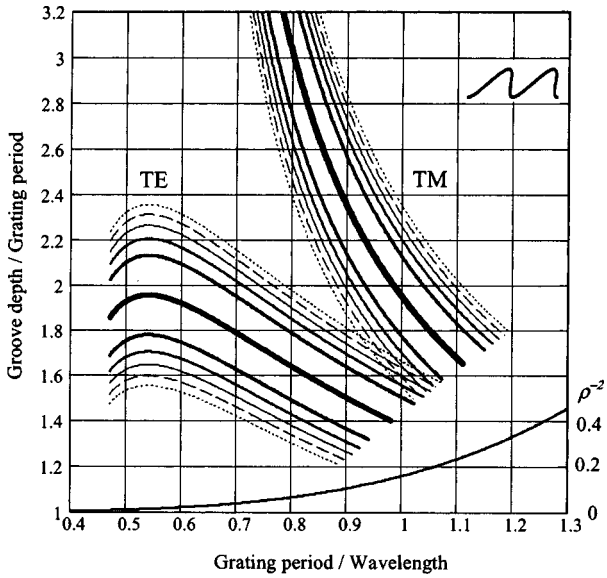

Fig. 9. Optimal aspect ratio h/Λ as a function of Λ/λ and their limits for different Bragg diffraction efficiencies η_{Bragg} for surface-relief gratings with sinusoidal slanted groove profile. Slant angle $\phi_s=17°$, refractive index of grooves $n_M=1.66$. ρ^{-2} is a two-wave criterion of Bragg diffraction regime with $\eta_{\text{Bragg}}=100\%$. Curves as in Fig. 8.

pect ratios would result in the same Bragg diffraction efficiency. The right lower ends of the curves indicate that for a certain aspect ratio h/Λ there is an upper bound Λ_{up} [Eq. (41)] for the grating period beyond which high Bragg diffraction efficiency cannot be obtained. Finally, the left ends of the curves indicate the subwavelength threshold Λ_{subw} [relation (15)] for the grating period. The results for ρ^{-2} indicate that the calculation errors of the effective grating model increase for larger normalized grating period Λ/λ.

The results of Figs. 8 and 9 can be exploited to design surface-relief gratings with high diffraction efficiency in TE as well as in TM polarization. As a first example, a Bragg diffraction efficiency of 98% with $\Lambda/\lambda=0.96$ can be obtained, for surface-relief gratings of sinusoidal groove profile with slant angle $\phi_s=17°$ and $n_M=1.66$, when the aspect ratio is $h/\Lambda=1.555$ with TE polarization and $h/\Lambda=1.897$ with TM polarization. To verify that these aspect ratios indeed result in high diffraction efficiencies, we calculated the diffraction efficiency of the +1st order as a function of incidence angle by using our effective grating model, and we compared the results with those obtained by numerical RCWA. The results are shown in Fig. 10. As evident, high diffraction efficiency is achieved, and there is a good agreement between the results of the effective grating model and numerical RCWA in the vicinity of the Bragg incidence angle $\theta_{inc,1}=8.8°$.

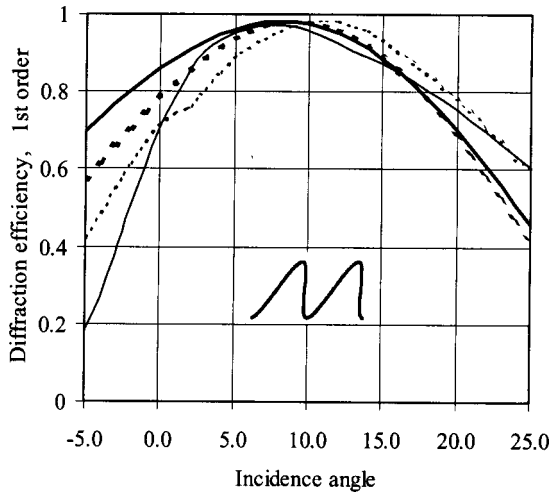

Fig. 10. The diffraction efficiency of the +1st order as a function of incidence angle for surface-relief gratings of sinusoidal slanted groove profile with angle $\phi_s=17°$. Optimal aspect ratio $h/\Lambda=1.555$ in TE polarization and $h/\Lambda=1.897$ in TM polarization lead to 98% diffraction efficiency at Bragg incident angle $\theta_{inc,1}=8.8°$. Refractive index of grooves $n_M=1.66$, $n_{sub}=1.52$, $\Lambda/\lambda=0.96$. Bold curves, effective-grating model; thin curves, numerical RCWA. Analytical: — TE, --- TM. Numerical: — TE, ----- TM.

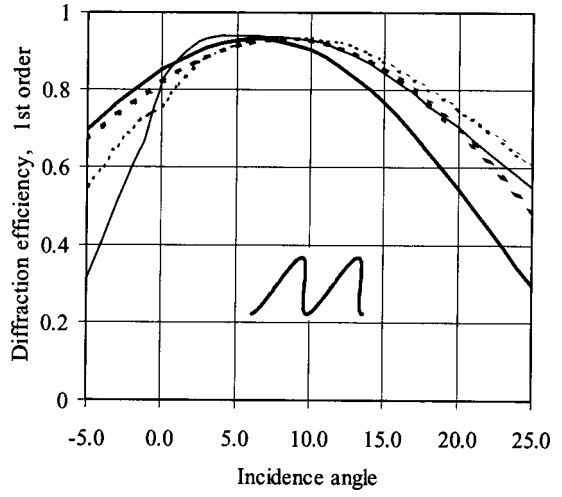

Fig. 11. Diffraction efficiency of the +1st order as a function of incidence angle for sinusoidal surface-relief gratings with aspect ratio $h/\Lambda=1.615$ optimized so as to achieve the same high diffraction efficiency of 93% for both TE and TM polarization at Bragg incident angle $\theta_{inc,1}=7.5°$. Slant angle is $\phi_s=17°$, $\Lambda/\lambda=1.0$, refractive index of grooves $n_M=1.66$, $n_{sub}=1.52$. Bold curves effective grating model; thin curves numerical RCWA. Curves as in Fig. 10.

As a second example, the same high Bragg diffraction efficiency of 93% for both TE and TM polarizations can be obtained, for a single surface-relief grating of sinusoidal groove profile with slant angle $\phi_s=17°$ and $n_M=1.66$, when $\Lambda/\lambda=1.0$ and the aspect ratio $h/\Lambda=1.615$. Again, to verify that this aspect ratio indeed results in high diffraction efficiencies, we calculated the diffraction efficiency of the +1st order as a function of incidence angle by using our effective grating model, and we compared the results with those obtained by numerical RCWA. The results are shown in Fig. 11. As evident, high diffraction efficiency is achieved, and there is a good agreement between the results of the effective grating model and numerical RCWA in the vicinity of the Bragg incidence angle $\theta_{inc,1}=7.5°$.

So far, a high diffraction efficiency has been obtained only at nonzero Bragg incidence angle in the cases of surface-relief gratings with symmetrical, moderately slanted, and sawtooth triangular groove profiles. For some applications, it is desired to obtain high diffraction efficiency at zero or at a specific Bragg incidence angle. Our calculations based on Eqs. (26), (36), and (37) reveal that, in general, this can be achieved by a rather unusual grating groove profile, with $q_c>1$. Such a q_c corresponds to an overhanging groove profile, where a part of one groove overlaps a part of the adjacent groove. As an example, we chose a surface-relief grating with triangular groove profile, $\Lambda/\lambda=1.1$, and $n_M=1.46$ and determined, from Eqs. (26) and (35)–(37), that $q_c=1.4$ is needed for obtaining Bragg incidence angle $\theta_{req}=0°$ while an aspect ratio of $h/\Lambda=2.091$ is needed for obtaining 100% Bragg diffraction efficiency with TE polarization. We then calculated the diffraction efficiency of the +1st diffraction order as a function of incidence angle for $q_c=1.4$, $q_c=1$, and $q_c=0.5$, all with its corresponding optimal aspect ratio. The results with our effective grating model as well as with numerical RCWA are presented in Fig. 12. As evident, a high diffraction efficiency of 100% can be achieved with all q_c, each at a different Bragg incidence angle; in particular, even at zero Bragg incidence angle for an overhanging groove profile with $q_c=1.4$. Also evident, again, is the close agreement between effective grating model calculations and numerical RCWA in the vicinity of the Bragg incidence angles.

6. CONCLUDING REMARKS

In this paper, we developed an effective grating model that explains the Bragg behavior of resonance domain

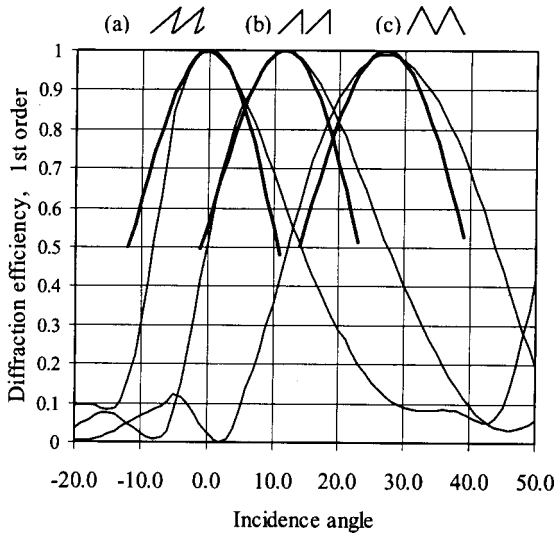

Fig. 12. The diffraction efficiency of the +1st order as a function of incidence angle, with aspect ratio h/Λ optimized for 100% diffraction efficiency at appropriate Bragg incident angles $\theta_{\mathrm{inc},1}$ for surface-relief gratings with triangular groove profiles at three different groove peak positions q_c: (a) overhanging of $q_c=1.4$, $h/\Lambda=2.091$, $\theta_{\mathrm{inc},1}=0.0°$, (b) sawtooth of $q_c=1.0$, $h/\Lambda=2.246$, $\theta_{\mathrm{inc},1}=11.7°$, and (c) symmetrical of $q_c=0.5$, $h/\Lambda=2.309$, $\theta_{\mathrm{inc},1}=27.0°$. Refractive index of grooves $n_M=1.46$, $n_{\mathrm{sub}}=1.46$, $\Lambda/\lambda=1.1$, and TE polarization. Bold curves, effective grating model; thin curves, numerical RCWA.

surface-relief gratings and provides analytic solutions for simplifying grating design and optimization. Specifically, a surface-relief grating in the resonance domain behaves similarly to a volume grating with graded refractive index, where the Bragg conditions must be satisfied. Thus such a grating could be modeled, in essence, by an effective sinusoidal graded-refractive-index grating whose groove slant angle depends on grating period, groove depth, groove material, and wavelength of the incident light. Our results reveal that to achieve high diffraction efficiency with surface-relief gratings, one must impose certain constraints in addition to the Bragg conditions. These constraints define an upper bound for the grating period at given groove depths. The effective grating model gives simple analytical relations for predicting and optimizing the performance of surface-relief gratings as a function of different parameters. Thus it is now possible to design diffractive optical elements in the resonance domain with the same simplicity as those in the scalar diffraction domain.

APPENDIX A: COUPLED-WAVE EQUATIONS FOR LIGHT PROPAGATION IN SUBLAYERS OF SLANTED SURFACE-RELIEF GRATINGS

After virtually splitting each groove in the surface-relief grating into a continuum of infinitesimally thin sublayers, we may expand the periodic function n^2 at each sublayer into an infinite complex Fourier series of "directional gratings" as

$$n^2=\sum_{\Delta j}[\Delta n_M^2 G_{\Delta j}(\zeta_r)+\bar{n}^2\delta_{\Delta j}]\exp(i\Delta j\mathbf{K}_r\mathbf{r}), \tag{A1}$$

with Fourier coefficients $G_{\Delta j}(\zeta_r)$ depending on the sublayer coordinate ζ_r within the groove depth and calculated in accordance with Eq. (7). Here $\delta_{\Delta j}=1$ when $\Delta j=0$, and $\delta_{\Delta j}=0$ when $\Delta j\neq 0$. Each term of expansion (A1) defines the directional graded-index gratings at the sublayer with given ζ_r and can be characterized with Fourier coefficients $G_{\Delta j}(\zeta_r)$ and their complex conjugates $G^*_{\Delta j}(\zeta_r)$. Note that the averaged refractive index $\bar{n}$ [Eq. (9)] and the grating vector $\mathbf{K}_r$ are the same in all the sublayers and coincide with those of the directionally averaged gratings. Now we consider the case of a unimodal grating profile. After simple analytical integration of the piecewise-constant function n^2 in Eq. (7), within the bounds of χ_{r1} to χ_{r2} for fixed ζ_r, the coefficients $G_{\Delta j}(\zeta_r)$ of a unimodal profile are found as

$$G_{\Delta j}(\zeta_r)=\Delta\chi_r\,\mathrm{sinc}(\Delta j\Delta\chi_r)\exp(-i2\pi\Delta j\chi_{rc})-\bar{g}\,\delta_{\Delta j}, \tag{A2}$$

where $\mathrm{sinc}(x)=\sin(\pi x)/(\pi x)$. The parameters of Eq. (A2) are shown in Fig. 2(b). Equation (A2) reveals that, in general, coefficients $G_{\Delta j}(\zeta_r)$ may have different phases, so the gratings of Eq. (A1) in sublayers with different ζ_r will not be matched in phase with each other. However, when the trajectory of the groove centers at each sublayer follows the angular orientation ϕ_r, as described by the equation

$$\chi_{rc}=0.5 \quad \text{or} \quad \chi_{r1}+\chi_{r2}=1, \tag{A3}$$

then the coefficients $G_{\Delta j}(\zeta_r)$ will have the same phase $-\pi\Delta j$ in sublayers with all ζ_r.

In each of the sublayers, the electric field $\mathbf{E}$ can be expanded, in accordance with the Floquet–Bloch theorem[21,23] in rotated coordinates x_r,y_r,z_r, into a Fourier series of coupled waves as

$$\mathbf{E}=\sum_{j=-\infty}^{\infty}\mathbf{e}_j S_j(z_r;\zeta_r)\exp(i\boldsymbol{\sigma}_j\mathbf{r}), \tag{A4}$$

where $\boldsymbol{\sigma}_j$ is defined in Eqs. (13) and (14), $\boldsymbol{\sigma}_j\mathbf{r}=k\bar{n}(s_{jr}x_r+c_{0r}z_r)$, and $\mathbf{e}_j=(e_{jxr},e_{jyr},e_{jzr})$, is the jth-order unit polarization vector, which is perpendicular to the plane of incidence for the case of TE polarization and parallel to it in the case of TM polarization. We now substitute Eqs. (A2) and (A4) into the generalized Helmholtz equation[1,27]

$$\nabla^2\mathbf{E}-\nabla(\nabla\cdot\mathbf{E})+k^2\bar{n}^2\mathbf{E}+k^2[n^2(x_r,z_r)-\bar{n}^2]\mathbf{E}=0. \tag{A5}$$

This leads to a set of second-order linear differential coupled-wave equations:

$$-\frac{i(1-e_{jzr}^2)}{2k\bar{n}c_{0r}}S_j''(z_r;\zeta_r)+S_j'(z_r;\zeta_r)=ik\bar{n}\sum_{j'}M_{j'-j}(\zeta_r)S_{j'}(z_r;\zeta_r), \tag{A6}$$

where "sublayer coefficients"

$$M_{jj'}(\zeta_r)=c_{0r}^{-1}[\kappa_{jj'}(\zeta_r)+\vartheta_j\delta_{j'-j}], \tag{A7}$$

with

$$\kappa_{jj'}(\zeta_r)=\delta n_M^2\mathbf{e}_j\cdot\mathbf{e}_{j'}G_{j'-j}(\zeta_r),$$

$$\vartheta_j=\tfrac{1}{2}(1-s_{jr}^2-c_{0r}^2), \tag{A8}$$

are constant within each sublayer but vary from sublayer to sublayer, $G_{j'-j}(\zeta_r)$ and δn_M^2 are defined in Eqs. (A2) and (25), respectively, and the prime and the double prime de-

note derivatives with respect to z_r.

We proceed, as usually done in the coupled-wave theory of gratings,[27,28] by neglecting the second-order derivatives in Eq. (A6). In particular, the eigenvalues of the Hermitian "sublayer matrix" $\mathbf{M}(\zeta_r)=[M_{j,j'}(\zeta_r)]$ must be much less than 1. This reduces Eq. (A6) to a simpler set of first-order differential coupled-wave equations

$$\mathbf{S}'(z_r;\zeta_r) = ik\bar{n}\mathbf{M}(\zeta_r)\mathbf{S}(z_r;\zeta_r) \tag{A9}$$

for vector $\mathbf{S}(z_r;\zeta_r)=[S_j(z_r;\zeta_r)]$ of complex amplitudes of diffraction orders, with a 2×2 sublayer matrix $\mathbf{M}(\zeta_r)=[M_{j,j'}(\zeta_r)]$. Note that our coupled-wave equations (A6) and (A9) as well as the Fourier expansion in Eq. (A1) are written in rotated coordinates rather than in the nonrotated coordinates usually exploited in RCWA.[14] From the theory of linear differential equations with constant coefficients, applied to Eq. (A9), we derive that the solution $\mathbf{S}(z_r+\Delta z_r;\zeta_r)$ at the exit (lower surface) of the sublayer is related to $\mathbf{S}(z_r;\zeta_r)$ at the entrance (upper surface) through multiplication of $\mathbf{S}(z_r;\zeta_r)$ by the exponential "transmittance matrix" $\mathbf{T}(\zeta_r;\Delta z_r)=\exp[ik\bar{n}\mathbf{M}(\zeta_r)\Delta z_r]$ for each sublayer, i.e., $\mathbf{S}(z_r+\Delta z_r;\zeta_r)=\mathbf{T}(\zeta_r;\Delta z_r)\mathbf{S}(z_r;\zeta_r)$. We note that $\mathbf{S}(z_r;\zeta_r)$ is continuous on the borders between sublayers because all the sublayers are embedded in the same medium with refractive index $\bar{n}$ and have the same propagation vectors $\boldsymbol{\sigma}_j$ and unit polarization vectors $\mathbf{e}_j$. Therefore $\mathbf{T}(\zeta_r;\Delta z_r)$ describes transformation of diffraction orders from the exit of the preceding sublayer to the exit of the current sublayer.

M. A. Golub can be reached by e-mail at michael.golub@weizmann.ac.il.

REFERENCES

1. M. Born and E. Wolf, *Principles of Optics* (Cambridge U. Press, Cambridge, UK, 1999).
2. D. H. Raguin and G. M. Morris, "Antireflection structured surfaces for the infrared spectral region," Appl. Opt. **32**, 1154–1167 (1993).
3. N. Bokor, R. Shechter, N. Davidson, A. A. Friesem, and E. Hasman, "Achromatic phase retarder by slanted illumination of a dielectric grating with period comparable with the wavelength," Appl. Opt. **40**, 2076–2080 (2001).
4. J. Turunen, M. Kuittinen, and F. Wyrowski, "Diffractive optics: electromagnetic approach," in *Progress in Optics, Vol. XL*, E. Wolf, ed. (Elsevier North-Holland, Amsterdam, 2000), pp. 343–388.
5. T. Shiono, T. Hamamoto, and K. Takahara, "High-efficiency blazed diffractive optical elements for the violet wavelength fabricated by electron-beam lithography," Appl. Opt. **41**, 2390–2393 (2002).
6. E. Noponen, A. Vasara, J. Turunen, J. M. Miller, and M. R. Taghizadeh, "Synthetic diffractive optics in the resonance domain," J. Opt. Soc. Am. A **9**, 1206–1213 (1992).
7. Y. Sheng, D. Feng, and S. Larochelle, "Analysis and synthesis of circular diffractive lens with local linear grating model and rigorous coupled wave theory," J. Opt. Soc. Am. A **14**, 1562–1568 (1997).
8. D. Meshulach, D. Yelin, and Y. Silberberg, "Adaptive real-time femtosecond pulse shaping," J. Opt. Soc. Am. B **15**, 1615–1619 (1998).
9. R. Shechter, Y. Amitai, and A. A. Friesem, "Compact beam expander with linear gratings," Appl. Opt. **41**, 1236–1240 (2002).
10. S. J. Walker, U. Jahns, L. Li, W. M. Mansfield, P. Mulgrew, D. M. Tennant, C. W. Roberts, L. C. West, and N. K. Ailawadi, "Design and fabrication of high-efficiency beam splitters and beam deflectors for integrated planar micro-optic systems," Appl. Opt. **32**, 2494–2501 (1993).
11. A. Sharon, D. Rosenblatt, A. A. Friesem, H. G. Weber, H. Engel, and R. Steingrueber, "Light modulation with resonant grating-waveguide structures," Opt. Lett. **21**, 1564–1566 (1996).
12. I. Nee, O. Beyer, M. Muller, and K. Buse, "Multichannel wavelength-division multiplexing with thermally fixed Bragg gratings in photorefractive lithium niobate crystals," J. Opt. Soc. Am. A **20**, 1593–1602 (2003).
13. G. W. Stroke, "Ruling, testing and use of optical gratings for high resolution spectroscopy," in *Progress in Optics, Vol. II*, E. Wolf, ed. (Elsevier North-Holland, Amsterdam, 1963), pp. 343–388.
14. M. G. Moharam and T. K. Gaylord, "Diffraction analysis of dielectric surface-relief gratings," J. Opt. Soc. Am. **72**, 1385–1392 (1982).
15. L. Li, "Multilayer modal method for diffraction gratings of arbitrary profile, depth, and permittivity," J. Opt. Soc. Am. A **10**, 2581–2591 (1993).
16. K. Yokomori, "Dielectric surface-relief gratings with high diffraction efficiency," Appl. Opt. **23**, 2303–2310 (1984).
17. D. M. Pai and K. A. Awada, "Analysis of dielectric gratings of arbitrary profiles and thicknesses," J. Opt. Soc. Am. A **8**, 755–762 (1991).
18. M. G. Moharam, D. A. Pommet, E. B. Grann, and T. K. Gaylord, "Stable implementation of the rigorous coupled wave analysis for surface-relief gratings: enhanced transmittance matrix approach," J. Opt. Soc. Am. A **12**, 1077–1086 (1995).
19. S. Peng and G. M. Morris, "Efficient implementation of rigorous coupled-wave analysis for surface-relief gratings," J. Opt. Soc. Am. A **12**, 1087–1096 (1995).
20. L. Li, J. Chandezon, G. Granet, and J.-P. Plumey, "Rigorous and efficient grating-analysis method made easy for optical engineers," Appl. Opt. **38**, 304–313 (1999).
21. R. Petit, ed., *Electromagnetic Theory of Gratings* (Springer-Verlag, Berlin, 1980).
22. E. Popov and E. G. Loewen, *Diffraction Gratings and Applications* (Marcel Dekker, New York, 1997), Chap. 4, Sect. 4.2.3.
23. M. Nevière and E. Popov, *Light Propagation in Periodic Media* (Marcel Dekker, New York, 2003).
24. H. J. Gerritsen, D. K. Thornton, and S. R. Bolton, "Application of Kogelnik's two-wave theory to deep, slanted, highly efficient, relief transmission gratings," Appl. Opt. **30**, 807–814 (1991).
25. M. A. Golub and A. A. Friesem, "Analytical theory for efficient surface relief gratings in the resonance domain," in *The Art and Science of Holography: A Tribute to Emmett Leith and Yuri Denisyuk*, H. J. Caulfield, ed. (SPIE Press, Bellingham, Wash., 2004), Chap. 19, pp. 307–328.
26. M. A. Golub, A. A. Friesem, and L. Eisen, "Bragg properties of efficient surface relief gratings in the resonance domain," Opt. Commun. **235**, 261–267 (2004).
27. H. Kogelnik, "Coupled wave theory for thick hologram gratings," Bell Syst. Tech. J. **48**, 2909–2947 (1969).
28. R. Magnusson and T. K. Gaylord, "Analysis of multiwave diffraction of thick gratings," J. Opt. Soc. Am. **67**, 1165–1170 (1977).
29. N. Chateau and J.-P. Hugonin, "Algorithm for the rigorous coupled-wave analysis of grating diffraction," J. Opt. Soc. Am. A **11**, 1321–1331 (1994).
30. J.-P. Plumey, B. Guizal, and J. Chandezon, "Coordinate transformation method as applied to asymmetric gratings with vertical facets," J. Opt. Soc. Am. A **14**, 610–617 (1997).
31. J. M. Miller, N. Beaucoudrey, P. Chavel, J. Turunen, and E. Cambril, "Design and fabrication of binary slanted surface-relief gratings for a planar optical interconnection," Appl. Opt. **36**, 5717–5727 (1997).
32. L. Li, "Oblique-coordinate-system-based Chandezon method for modeling one-dimensionally periodic, multilayer, inhomogeneous, anisotropic gratings," J. Opt. Soc. Am. A **16**, 2521–2531 (1999).
33. P. Laakkonen, M. Kuittinen, J. Simonen, and J. Turunen,

"Electron-beam-fabricated asymmetric transmission gratings for microspectroscopy," Appl. Opt. **39**, 3187–3191 (2000).
34. M. G. Moharam, T. K. Gaylord, and R. Magnusson, "Criteria for Bragg regime diffraction by phase gratings," Opt. Commun. **32**, 14–18 (1980).
35. M. Breidne and D. Maystre, "Equivalence of ruled, holographic, and lamellar gratings in constant deviation mountings," Appl. Opt. **19**, 1812–1821 (1980).
36. M. A. Golub, "Generalized conversion from the phase function to the blazed surface-relief profile of diffractive optical elements," J. Opt. Soc. Am. A **16**, 1194–1201 (1999).